RSC Advances

ROYAL SOCIETY OF CHEMISTRY

www.rsc.org/advances

Synthesis of Ni/Au/Co Trimetallic Nanoparticles and Their Catalytic Activity for Hydrogen Generation from Alkaline Sodium Borohydride Aqueous Solution

Chengpeng Jiao [a], Zili Huang [a], Xiaofeng Wang [a], Haijun Zhang [b*], Lilin Lu [c], Shaowei Zhang [b]

[a] *Hubei Key Laboratory for Efficient Utilization and Agglomeration of Metallurgical Mineral Resources, Wuhan University of Science and Technology, Wuhan 430081, China*

[b] *The State Key Laboratory of Refractories and Metallurgy, Wuhan University of Science and Technology, Wuhan 430081, China*

[c] *College of Chemical Engineering and Technology, Wuhan University of Science and Technology, Wuhan 430081, China*

*Corresponding author; E-mail: zhanghaijun@wust.edu.cn.

*Corresponding author, Prof. Dr. Haijun Zhang (Telephone number: +86-27-68862829, Fax: +86-27-68862829, E-mail: zhanghaijun@wust.edu.cn). Corresponding address: Prof. Haijun Zhang, Mail box No. 121, College of Materials and Metallurgy, Wuhan University of Science and Technology, No.947 Heping Road, Wuhan, Hubei Province, P. R. China

Abstract

A series of Poly (N-vinyl-2-pyrrolidone) stabilized colloidal Ni/Au/Co trimetallic nanoparticles (TNPs) were synthesized by co-reduction of corresponding metal precursors via dropwise addition of $NaBH_4$. Ultraviolet-visible spectrophotometry (UV-Vis), X-ray photoelectron spectroscopy (XPS), transmission electron microscopy (TEM), powder X-ray diffraction (XRD) and high-resolution transmission electron microscopy (HR-TEM) equipped with energy dispersive spectrometer (EDS) were combined to characterize the morphology, crystalline structure and electron distribution of the as-prepared TNPs. The effects of metal compositions on size distribution and hydrogen generation from catalytic hydrolysis of alkaline $NaBH_4$ aqueous solutions were also investigated. The results indicated that as-prepared alloy-structured $Ni_{45}Au_{45}Co_{10}$ TNPs showed the maximum catalytic activity of 1170 mol-H_2/(h mol-M), which is several times higher than that of the as-prepared Au, Ni or Co monometallic nanoparticles (MNPs), or $Au_{50}Ni_{50}$, $Au_{50}Co_{50}$ or $Ni_{50}Co_{50}$ bimetallic nanoparticles (BNPs). The enhanced catalytic activity of the TNPs compared with the MNPs and BNPs could be attributed to the presence of electron charge transfer effects among Au, Ni and Co atoms, which is supported by the result of X-ray photoelectron spectroscopy (XPS) and density functional theory (DFT) calculation. The apparent activation energy of the as-prepared $Au_{45}Ni_{45}Co_{10}$ TNPs in hydrolysis of $NaBH_4$ aqueous solution was determined as 18.8 kJ/mol.

Keywords: Ni/Au/Co; Trimetallic nanoparticle; Alloy; Catalytic activity; Hydrogen generation

1. Introduction

During the past decade, chemical hydrogen storage materials have attracted a great deal of attention since they can release large amount of hydrogen gas at ambient temperature and thus act as a new source for producing hydrogen [1-5]. Comparing with other chemical hydrogen storage materials such as ammonia borane (NH_3BH_3) and hydrazine hydrate ($N_2H_4 \cdot H_2O$), sodium borohydride ($NaBH_4$) is more competitive because of its several advantages such as easier control in the hydrogen generation rate and hydrogen purity[6], the safer production process, the recyclability of byproduct $NaBO_2$ to borohydride[7], and the lower hydrogen releasing temperature[8].

Noble metal nanoparticles (NPs) such as Pt[9, 10], Pd[11, 12], Ru[13-15] and Rh[16-18] are conventionally used as catalysts for hydrogen generation. However, the relatively high cost and the limited reservation of the precious metals hindered their further industrial applications. Recently, cost-effective transition metal NPs, such as Fe, Co and Ni, have been developed as alternatives to noble metal catalysts for hydrogen generation [19-21]. For example, Busca, *et al.* [22] reported that cubic structured cobalt NPs could be used as active and selective catalyst for ethanol steam reforming reaction, and ÖZdemir, *et al.* [23] found a high catalytic performance of Co/B catalysts in hydrogen generation from hydrolysis of $NaBH_4$ solution. In addition, many researches discussed the effects of preparation condition, support's type and protective agents on morphologies and catalytic activities of Co NPs in hydrogen generation [24-26].

Bi- and tri-metallic nanoparticles (BNPs and TNPs) were reported to be more active in chemical reactions than their counterparts of monometallic nanoparticles (MNPs) because of the so-called lattice strain effects, geometric effects and electronic charge transfer effects[27, 28]. It was

also demonstrated that alloying of noble metals with other non-noble transition metals not only led to the enhanced catalytic performance but also reduced the overall cost [29]. For instance, according to Jiang et al. [30], Ag_{10}/Co_{90} BNP catalysts exhibited a five times greater catalytic activity than Co catalysts in hydrolysis of $NaBH_4$ solution. Kargupta, *et al.* [31] reported a highly active and stable graphene supported bimetallic Co/Pt nanohybrid for hydrogen generation from $NaBH_4$ solution. And our group [32] found that the catalytic activity of alloy-structured $Au_{50}Ni_{50}$ BNPs in hydrogen generation from the hydrolysis of $NaBH_4$ was several times higher than that of corresponding Au and Ni MNPs.

Although much less work has been done to date on the synthesis and catalytic activity of TNPs comparing with the case of BNPs, it should be pointed that the studies on the former have been increasing rapidly, especially, during the past few years. For example, Chan *et al.* [33] found that Pt/Fe/Ni trimetallic nanocatalysts with ultralow Pt loading showed a much better oxygen reduction reaction (ORR) activity in fuel cells than a pure Pt electrode catalyst. On the other hand, $Au_{60}Pt_{10}Pd_{30}$ TNPs were reported to show a better catalytic activity for the glucose oxidation than their counterparts of MNPs and BNPs[34]. Furthermore, core/shell structured-Pd/Co@Pt TNPs were found to show a greatly improved electrocatalytic performance in the ORR compared to commercial Pt/C catalyst [35]. Ni/Ag/Pd and $Ni_{40}Au_{15}Pd_{45}$ TNPs were reported to be catalytically effective, achieving nearly 100% selectivity in the dehydrogenation of formic acid [36, 37]. In addition, Basu *et al.* [38] revealed that $Ir_5Pt_{20}Sn_{15}/C$ electro-catalysts exhibited higher activity towards ethanol oxidation than the corresponding BNPs.

Herein, we report a facile one-pot approach to the preparation of PVP (poly (N-vinyl-2-pyrrolidone)) stabilized colloidal Ni/Au/Co TNPs catalysts using $NaBH_4$ as a reduction agent for the first time. The effects of atomic ratios on the size distribution and catalytic

activity in hydrogen generation from alkaline $NaBH_4$ solutions were also examined. It was demonstrated that as-prepared alloy-structured $Ni_{45}Au_{45}Co_{10}$ TNPs with an average diameter of 1.9 ± 0.6 nm showed much greater catalytic activity in hydrogen generation than the corresponding MNPs and BNPs. The corresponding apparent activation energy of $Ni_{45}Au_{45}Co_{10}$ TNPs for hydrogen generation was also determined by using the Arrhenius method.

2. Experimental Section

2.1 Raw Materials

Hydrogen tetrachloroaurate tetrahydrate ($HAuCl_4 \cdot 4H_2O$, 99.9%), cobalt (II) chloride hexahydrate ($CoCl_2 \cdot 6H_2O$, 99%), nickel (II) chloride hexahydrate ($NiCl_2 \cdot 6H_2O$, 99.0%), sodium borohydride ($NaBH_4$, 96.0%), PVP (K30, average molecular weight of about 30, 000), and sodium hydroxide (NaOH, 96.0%) purchased from Sinopharm Ltd., were used directly as the main starting materials without further purification.

2.2 Preparation of PVP-stabilized Ni/Au/Co TNPs

PVP-stabilized Ni/Au/Co TNPs were prepared by adding $NaBH_4$ dropwise to a mixture of the corresponding metal precursors. For example, $Ni_{50}Au_{10}Co_{40}$ TNPs (Hereafter, the numbers in the subscript denote the feeding ratio of the corresponding metal ions) were prepared as follows: aqueous solutions of $NiCl_2 \cdot 6H_2O$ (25 mL, 0.66 mM), $HAuCl_4 \cdot 4H_2O$ (5 mL, 0.66 mM) and $CoCl_2 \cdot 6H_2O$ (20 mL, 0.66 mM) were added to an aqueous PVP solution (50 mL, 66 mM in monomer unit; R_{PVP}=100, R_{PVP} is defined as the molar ratio of PVP in monomer units to the total metal ions) in a 250 mL two-neck flask and then stirred for 30 min at 0℃. This was followed by addition of an aqueous solution of $NaBH_4$ (10 mL, 16.5 mM, 0℃; R_{NaBH4}=5, R_{NaBH4} is defined as the molar ratio of $NaBH_4$ to the total metal ions) at a rate of one drop per 3 seconds to the mixed

solution under vigorous stirring. And finally the colloidal dispersions of Ni/Au/Co TNPs were obtained after further 1 h stirring at 0℃.

2.3 Characterization of Nanoparticles

Ultraviolet and visible light (UV-Vis) absorption spectra were recorded over 200-800 nm using a Shimadzu 2550 recording spectrophotometer equipped with a quartz cell with an optical path length of 10 mm. Transmission electron microscopy (TEM) images were taken at the accelerated voltage of 80 kV using an FEI Tecnai G^2 50-S-TWIN TEM. The samples were obtained by dropping one or two droplets of the prepared colloidal ethanol solution onto a copper microgrid covered with a thin amorphous carbon film and followed by evaporating the water in air at room temperature. For each sample, generally at least 200 particles from different locations on the grid were selected to evaluate the mean diameter. High-resolution transmission electron microscopy (HR-TEM) images were taken at the accelerated voltage of 200 kV using a JEM-2100F Field Emission High-resolution TEM. Powder X-ray diffraction (XRD) analysis of powder TNPs was carried out on D/MAX-RB RU-200B rotation anode high power X-ray diffractormeter (Cu Kα radiation at a scanning rate of 0.026° s^{-1}, room temperature). All the image analyses were processed by using the iPP software package. X-ray photoelectron spectroscopy (XPS) measurement was performed using a Quantum 2000 spectrometer with Al Kα radiation. Binding energies (BE) were normalized by taking the C (1s) BE of adventitious carbon contamination as 284.6 eV, and the analyses on Au were based on $Au4f_{5/2}$ and $Au4f_{7/2}$ peaks.

2.4 Catalytic Activity of Ni/Au/Co TNPs

The catalytic activity of as-prepared colloidal NPs was evaluated based on the volume of hydrogen generated from hydrolysis of an alkaline $NaBH_4$ solution. Experiments were carried out in a two-necked round-bottom flask with one opening connected to a gas burette and the other to

an addition funnel with a pressure-equalization arm. The volume of H_2 generated was measured by the displacement level of water in a burette at room temperature, and the temperature for the activity evolution was maintained at 30 ℃ using a water bath. All the catalytic experiments were carried out after vigorous stirring of the quantified colloidal catalysts for 10 min to remove the residual H_2 in the solution and to minimize the temperature difference between the colloidal catalyst and the water bath. In all catalytic activity tests, the molar ratio of metals in the colloidal catalyst mixture (40 mL) to the $NaBH_4$ in alkaline solution (10 mL, 30 mM, pH 12) was controlled at 0.05.

In the reusability evaluation of the as-prepared TNPs, the catalyst was re-used immediately in a new batch after the previous test. A new basic $NaBH_4$ aqueous solution (10 mL, 30 mM and pH 12) was added into the flask to regenerate hydrogen. Such cycle was repeated 7 times under ambient atmosphere at 30 ℃.

2.5 Density Functional Theory (DFT) Calculation

First-principles calculations were performed with the density functional theory (DFT) using the Dmol^3 program [39]. All electron relativistic core treatment and doubled numerical basis set with polarization functions, along with the Perdew-Burke-Ernzerhof (PBE) [40] generalized gradient approximation (GGA) exchange-correlation functions were used to perform full optimization of the investigated $Ni_{25}Au_6Co_{24}$ model clusters without symmetry constraint. Spin-restricted self-consistent-field (SCF) calculations were carried out with SCF convergence criterion set to the root-mean-square change in the electronic density less than of 10^{-5} eV. The convergence criteria applied for geometry optimization were enforced to 0.00002 au for energy, 0.004 au/Å for force, and 0.005 Å for maximum displacement. Mulliken population analysis was performed to investigate the atomic charges distribution.

3. Results and Discussion

3.1 Structure and Catalytic Activity of Ni/Au/Co TNPs

Our previous results indicated that alloy-structured $Ni_{50}Au_{50}$ BNPs prepared by dropwise addition of $NaBH_4$ showed several times higher catalytic activity for hydrogen generation from the hydrolysis of $NaBH_4$ aqueous solution than corresponding Au and Ni MNPs[32]. Nevertheless, it is still far from practical application considering the relatively high Au content (50 atom %) in such Au-containing catalysts and their not-high-enough catalytic activity (800 mol-H_2/(h·mol-M)). Thus, partial substitution of Au by Co to prepare Ni/Au/Co TNPs was firstly investigated in this work by keeping the Ni content at 50 atom % and varying the Co content from 20 to 40 atom %. Au, Ni, Co, $Ni_{50}Au_{50}$, $Ni_{50}Au_{30}Co_{20}$ and $Ni_{50}Au_{10}Co_{40}$ NPs were prepared by dropwise addition of $NaBH_4$ under identical conditions of $[M^{n+}]$ = 0.66 mM, R_{NaBH4}=5, and R_{PVP}=100. The UV-Vis spectra of as-prepared NPs are shown in Fig. 1. The spectrum of Au MNPs exhibits a plasmon absorbance peak around 520 nm which is consistent with those reported previously [41-43]. On the other hand, the spectrum of aqueous dispersed Ni and Co MNPs displays a featureless and monotonically increasing absorbance toward shorter wavelength. In the case of the prepared TNPs, the overall absorbance strength dampens with increasing the Co contents from 20 to 40 atom%, suggesting the different compositions of the TNPs. And the obvious differences between the spectra of the $Ni_{50}Au_{30}Co_{20}$ and $Ni_{50}Au_{10}Co_{40}$ TNPs and those of the corresponding MNPs and BNPs indicate that the composition of the formed TNPs were different from that of MNPs or BNPs. It can be reasonably deduced that the as-prepared colloidal TNP catalysts are alloy-structured since the suppression of the Au plasmon peaks was evidently observed with Au content decreasing.

TEM images were taken to characterize the average size and size distributions of the prepared NPs, a representative set of TEM images along with size distribution histograms are shown in Fig. 2. The average particle sizes of Au, $Ni_{50}Au_{50}$, $Co_{50}Au_{50}$, $Ni_{50}Au_{30}Co_{20}$ and $Ni_{50}Au_{10}Co_{40}$ NPs are 3.0 ± 1.3 nm, 2.7 ± 0.8 nm, 2.8 ± 1.1 nm, 1.5 ± 0.4 nm and 2.1 ± 0.5 nm, respectively. It can be concluded that the average sizes of all the evenly dispersed spherical TNPs with a relatively narrower size distribution are smaller than those of the prepared Au MNPs, and $Ni_{50}Au_{50}$ and $Co_{50}Au_{50}$ BNPs. In the cases of Co and Ni MNPs, our results (TEM not shown here) revealed that it is difficult to prepare them with a very small size by using the present $NaBH_4$ reduction method. As a result, Co and Ni NPs with an average size of about several tens nanometers were obtained. These results confirmed that TNPs rather than physical mixtures of Au, Ni and Co MNPs or mixtures of MNPs and BNPs were obtained.

To further investigate the structure of the as-prepared TNPs, crystallographic lattice fringe analysis based on HR-TEM images of $Ni_{50}Au_{10}Co_{40}$ was also carried out. As shown in Fig. 3, for particle-1 and particle-3, the measured average interplanar distances of 0.217 nm and 0.218 nm did not match with any face in pure Au, Ni or Co NPs. However, the measured average interplanar distances of the TNPs were between the interplanar distances of (111) face of Ni (0.1992 nm; Ni: JCPDS 88-2326), Co (0.2047nm; Co: JCPDS 15-0806) and Au (0.2355nm; Au: JCPDS 89-3697). Similarly, the interplanar distances of 0.133 nm and 0.185 nm for particle-2 and particle-4 lie between the lattice spacing of (220) and (200) face of Ni (0.1220 nm for 220 face and 0.1725 nm for 200 face; Ni: JCPDS 88-2326), Co (0.1253 nm for 220 face and 0.1772 nm for 200 face; Co: JCPDS 15-0806) and Au (0.1442 nm for 220 face and 0.2040 nm for 200 face; Au: JCPDS 89-3697) respectively. These results further confirmed that alloy-structured TNPs were formed and the formation of individual Au, Co and Ni MNPs in the as-prepared NPs can be ruled

out. XRD was also used to characterize the structure of the prepared TNPs (Fig. S1). It showed that 2 diffraction peaks at 2θ=38.42° and 44.68° can be observed in the XRD spectrum of the $Ni_{45}Au_{45}Co_{10}$ TNPs (Fig. S1). Further analysis proved that the peaks centered at 38.42° and 44.68° are not well in consistent with the (111) and (200) face of the bulk Au (38.179° and 44.375°, respectively; Au: JCPDS 89-3697). It seems that they are located among the corresponding diffraction peak of the three corresponding monometallic nanoclusters (Table S1), this result is also in agreement with the results of the HRTEM in Fig. 3.

The catalytic activities of the as-prepared Au, Ni, Co, $Ni_{50}Au_{50}$, $Co_{50}Au_{50}$, $Ni_{50}Co_{50}$, $Ni_{50}Au_{30}Co_{20}$ and $Ni_{50}Au_{10}Co_{40}$ NPs in hydrogen generation from alkaline $NaBH_4$ solution were evaluated and compared (shown in Fig. 4). Although the prepared TNPs did not show higher activity for hydrogen generation (about 790 mol-H_2/(h·mol-M)) than $Ni_{50}Au_{50}$ (about 800 mol-H_2/(h·mol-M)), however, it should be pointed out that the prepared $Ni_{50}Au_{10}Co_{40}$ and $Ni_{50}Au_{30}Co_{20}$ TNPs are much cheaper catalysts for hydrogen generation from alkaline $NaBH_4$ solution than $Ni_{50}Au_{50}$ BNPs taking the Au % into consideration.

It is well known that the catalytic activity of NPs is determined by its structure and composition. To get a thorough understanding of the effect of composition on the particle size and catalytic activity of the Ni/Au/Co TNPs in hydrogen generation, another series of $Ni_{(50-x/2)}Au_{(50-x/2)}Co_x$ (x=10, 20, 30, 40) TNPs were also synthesized by varying the Co content while fixing the Au: Ni (atom%) at 1: 1 (this was because our previous results showed that the $Ni_{50}Au_{50}$ NPs possessed the highest catalytic activity in all the prepared Ni/Au BNPs [32]). The corresponding UV-Vis spectra of the prepared TNPs (Fig. 5) show that the spectra are similar to those of the $Ni_{50}Au_{30}Co_{20}$ and $Ni_{50}Au_{10}Co_{40}$ TNPs synthesized earlier. The suppression of the characteristic absorption peak of Au NPs at 520 nm with the reducing of Au content indicated

again that alloy-structured Ni/Au/Co TNPs were formed, which is in agreement with the results in Figs. 1-4.

The average particle sizes based on TEM images of $Ni_{30}Au_{30}Co_{40}$, $Ni_{35}Au_{35}Co_{30}$, $Ni_{40}Au_{40}Co_{20}$ and $Ni_{45}Au_{45}Co_{10}$ TNPs were determined as 3.1 ± 0.6 nm, 3.1 ± 0.9 nm, 2.5 ± 0.6 nm and 1.9 ± 0.6 nm, respectively (Fig. 6). The catalytic activities of the TNPs were also evaluated for the hydrolysis of alkaline $NaBH_4$ aqueous solution. The results indicated that the $Ni_{45}Au_{45}Co_{10}$ TNPs showed the highest catalytic activity of 1170 mol-H_2/(h·mol-M) (Fig. 7) which was about 1.5, 8, 10 and 14 times greater than that of $Ni_{50}Au_{50}$ BNPs, Au, Ni and Co MNPs respectively (Fig. 4, Table S2), and at least 2.5 times greater than that of the physically mixed catalyst of Au and Ni MNPs in the molar ratio of 50/50 [44]. These results suggested once again that the prepared NPs were Ni/Au/Co TNPs, not physical mixtures of the corresponding MNPs and/or BNPs.

The reusability of the $Ni_{45}Au_{45}Co_{10}$ TNPs for hydrogen generation from alkaline $NaBH_4$ was also investigated. The catalyst was re-used immediately in a new batch after the previous test. The catalytic activity of $Ni_{45}Au_{45}Co_{10}$ TNPs sharply decreased after use in the first run, and about 60% and 25% of the initial catalytic activity were maintained after the first and seventh cycles, as shown in Fig. S2-3. The deactivation of the $Ni_{45}Au_{45}Co_{10}$ TNPs can be ascribed to the agglomeration of the TNPs after the catalytic reaction, and the agglomeration can be clearly observed from the TEM images shown in Fig. S4 which demonstrated that the originally well dispersed colloidal $Ni_{45}Au_{45}Co_{10}$ TNPs were got together after seven catalytic runs. Although the reusability of the prepared TNPs is still far from satisfying, it should be pointed out that, to the best of our knowledge, this has been the first report to date on the preparation and catalytic activity of Ni/Au/Co TNPs for hydrogen generation from hydrolysis of $NaBH_4$.

Moreover, the effect of temperature on the catalytic activity of the as-prepared TNPs was also investigated using $Ni_{45}Au_{45}Co_{10}$ and $Ni_{50}Au_{10}Co_{40}$ as example catalysts. The catalytic properties were enhanced with increasing the reaction temperature. And the apparent activation energy (E_a) of the PVP-protected $Ni_{45}Au_{45}Co_{10}$ TNPs in hydrogen generation from the hydrolysis of alkaline $NaBH_4$ solution was calculated by using the Arrhenius method (Fig. 8). The slope of the linear plot between the natural logarithm of the temperature-dependent rate constant and the inverse of temperature is E_a/R, where R is the universal gas constant. In terms of the Arrhenius plots within the temperatures range from 303 to 318 K, E_a was calculated to be 18.8 kJ/mol for $Ni_{45}Au_{45}Co_{10}$ and 91.6 kJ/mol for $Ni_{50}Au_{10}Co_{40}$ TNPs (Fig. 8 and Fig. S5). For comparison, the E_a values of $Ni_{50}Au_{50}$[32], Co/Cu/α-Al_2O_3 [45], Ni/Fe-B[30], Ru/montmorillonite[46], Co/Ru-B[47], Co-P[48] and Au/Co-Ti[49] catalysts were reported to be 30.3 kJ/mol, 52 kJ/mol, 57 kJ/mol, 54.7 ±1 kJ/mol, 48.8 kJ/mol, 48.1 kJ/mol and 37.9 kJ/mol respectively. These results suggested that the $Ni_{45}Au_{45}Co_{10}$ TNPs prepared in this work were excellent catalysts for the hydrolysis of $NaBH_4$.

3.2 Correlation between Catalytic Activity of the TNPs and the Electronic Structure

The higher catalytic activity of the Ni/Au/Co TNPs than that of the corresponding MNPs and BNPs could be attributed to the effects of electronic charge transfer between Ni, Au and Co atoms. Such effects were confirmed previously to be responsible for the high catalytic activities of several types of BNPs [50-52] and TNPs[34]. It can be reasonable deduced that there exist at least three types of charge transfer effects in the prepared Ni/Au/Co TNPs due to the differences in the ionization energy values (Ni: 7.63 eV; Au: 9.22 eV; and Co: 7.86 eV;): 1) charge transfer from individual Co atoms to Au atoms; 2) charge transfer from individual Ni atoms to Au atoms; and 3) electron donation from Ni to Co and then to Au atoms. The possible electronic charge transfer routes in Ni/Au/Co TNPs are illustrated in Fig. 9. The negatively charged Au and Co atoms, and

positively charged Ni atoms resulted from the electron charge transfer effects can act as the catalytic active sites for the hydrogen generation from alkaline $NaBH_4$ aqueous solution. In can be considered that the negatively charged Au and Co atoms may facilitate the breaking of the H-O bonds in H_2O molecules, in which the two hydrogen atoms are in one-positive-valence. On the other hand, the positively-charged Ni atoms may promote the breaking of the B-H chemical bonds in $NaBH_4$ molecules. And then a hydrogen molecule is formed via combination of the two hydrogen atoms produced from H_2O and $NaBH_4$ molecules, respectively. We consider that the enhanced catalytic activity of the TNPs could be resulted from the synergetic effect between the charged Ni, Au and Co atoms and $NaBH_4/H_2O$ molecule.

To confirm the electronic charge transfer effects and the presence of the negatively charged Au and Co atoms and positively charged Ni atoms in the TNPs, the electronic characteristics of the surface atoms of $Ni_{50}Au_{10}Co_{40}$ TNPs were investigated by using high-resolution XPS with monochromated Al K_α electron radiation. The $Ni_{50}Au_{10}Co_{40}$ TNPs stabilized by low content of PVP (R_{PVP}=5) were prepared for the characterization. XPS results (shown in Fig. S6) showed that the electron apparent BE of Au $4f_{7/2}$ was 83.85 eV for the $Ni_{50}Au_{10}Co_{40}$ TNPs, this is about 0.10 eV lower than that in bulk Au (83.95 eV). This result provided a direct evidence for the presence of the negatively charged Au atoms in the TNPs. As for Ni and Co atoms, the electron BE values of Ni $2p_{3/2}$ and Co $2p_{3/2}$ were 855.80 eV and 781.05 eV, respectively, suggesting the formation of Ni^{2+} and Co^{2+} ions. The formation of Ni^{2+} and Co^{2+} ions can be attributed to the oxidation of the TNPs during the XPS measurement. Even so, it can be still considered that Ni, Au and Co atoms in the TNPs play dominant roles in the catalytic activity for hydrogen generation from $NaBH_4$ solution considering that the preparation of the TNPs was carried out in a N_2 atmosphere, and the TNPs in all the catalytic activity tests were protected by a sufficient amount of PVP (R_{PVP}=100).

The electronic charge transfer effects and the existence of negatively charged Au and Co atoms, and positively charged Ni atoms in the synthesized TNPs were further confirmed by the DFT calculations of M_{55} model NPs with the composition of $Ni_{25}Au_6Co_{24}$ (whose composition is similar to that of the $Ni_{50}Au_{10}Co_{40}$ TNPs). As seen from Fig. 10, the Au and Co atoms in the M_{55} model are indeed negatively charged, whereas the Ni atoms are positively charged. The DFT calculation results suggest again the presence of electronic charge transfer effects among Au, Ni and Co atoms in the TNPs.

4. Conclusions

A series of PVP-protected $Ni_{50}Au_xCo_{50-x}$ and $Ni_{(50-x/2)}Au_{(50-x/2)}Co_x$ (x=10, 20, 30, 40) TNPs with an alloyed structure were synthesized by co-reduction of corresponding metal precursors via dropwise addition of $NaBH_4$ solution. Among the corresponding MNPs, BNPs and TNPs, as-prepared $Ni_{45}Au_{45}Co_{10}$TNPs exhibited the highest catalytic activity with a value of 1170 mol-H_2/(h mol-M) in hydrogen generation from hydrolysis of $NaBH_4$. This could be attributed to the presence of negatively charged Au and Co atoms and positively charged Ni atoms, which was confirmed by both XPS and DFT calculations. The apparent activation energy of the prepared $Ni_{45}Au_{45}Co_{10}$ TNPs in hydrolysis of $NaBH_4$ aqueous solution was determined as 18.8 kJ/mol.

Acknowledgements

This work was financially supported by National Natural Science Foundation of China (General program, 51272188, 51472184, 51472185), State Basic Research Development Program of China (973 Program, 2014CB660802), Natural Science Foundation of Hubei Province, China (Contract No. 2013CFA086) and Foreign cooperation projects in Science and Technology of

Hubei Province, China (Contract No. 2013BHE002).

References

1 A. Hamaed, T.K.A. Hoang, G. Moula, R. Aroca, M.L. Trudeau, D.M. Antonelli, *J. Am. Chem. Soc.*, 2011, **133** (39), 15434.

2 R. Moury, U.B. Demirci, V. Ban, Y. Filinchuk, T. Ichikawa, L. Zeng, K. Goshome, P. Miele, *Prog. Aerosp. Sci.*, 2013, **60**, 45.

3 C.Y. Duan, H. Wang, X.M. Ou, F. Li, X.H. Zhang, *ACS Appl. Mater. Inter.*, 2014, **6** (12), 9742.

4 G. Cipriani, V. Di-Dio, F. Genduso, D. La-Cascia, R. Liga, R. Miceli, G. Ricco-Galluzzo, *Int. J. Hydrogen Energy*, 2014, **39**(16), 8482.

5 K.P. Brooks, T.A. Semelsberger, K.L. Simmons, B. van-Hassel, *J. Power Sources*, 2014, **268**, 950.

6 P.J.R. Pinto, T. Sousa, V.R. Fernandes, A.M.F.R. Pinto, C.M. Rangel, *Int. J. Elec. Power*, 2013, **49**, 57.

7 T. Ou, A. Barbucci, P. Carpanese, S. Congiu, M. Panizza, *Int. J. Hydrogen Energy*, 2014, **39**(21), 11094.

8 J.H. Wee, K.Y. Lee, S.H. Kim, *Fuel Process. Technol.*, 2006, **87**(9), 811.

9 L. He, Y.Q. Huang, A.Q. Wang, Y. Liu, X.Y. Liu, X.W. Chen, J.J. Delgado, X.D. Wang, T. Zhang, *J. Catal.*, 2013, **298**, 1.

10 C. Lucarelli, S. Albonetti, A. Vaccari, C. Resini, G. Taillades, J. Roziere, K.E. Liew, A. Ohnesorge, C. Wolff, I. Gabellini, D. Wails, *Catal. Today*, 2011, **175**(1), 504.

11 Y. Tong, X.F. Lu, W.N. Sun, G.D. Nie, L. Yang, C. Wang, *J. Power Sources,* 2014, **261**, 221.

12 C.Q. Hu, J.K. Pulleri, S.W. Ting, K.Y. Chan, *Int. J. Hydrogen Energy*, 2014, **39**(1), 381.

13 C. Crisafulli, S. Scirè, M. Salanitri, R. Zito, S. Calamia, *Int. J. Hydrogen Energy*, 2011, **36**(6), 3817.

14 X.J. Li, G.Y. Fan, C.M. Zeng, *Int. J. Hydrogen Energy*, 2014, **39**(27), 14927.

15 Y.H. Li, Q. Zhang, N.W. Zhang, L.H. Zhu, J.B. Zheng, B.H. Chen, *Int. J. Hydrogen Energy*, 2013, **38**(30), 13360.

16 F. Gunnarsso, M.Z. Granlund, M. Englund, J. Dawody, L.J. Pettersson, H. Härelind, *Appl. Catal. B-Environ.*, 2015, **162**, 583.

17 Y. Zhang, D.A.J.M. Ligthart, X.Y. Quek, L. Gao, E.J.M. Hensen, *Int. J. Hydrogen Energy*, 2014, **39**(22), 11537.

18 M. Rakap, *Appl. Catal. B-Environ.*, 2015, **163**, 129.

19 J. Zhu, R. Li, W.L. Niu, Y.J. Wu, X.L. Gou, *Int. J. Hydrogen Energy*, 2013, **38**(25), 10864.

20 L.J. Jin, H.H. Si, J.B. Zhang, P. Lin, Z.Y. Hu, B. Qiu, H.Q. Hu, *Int. J. Hydrogen Energy*, 2013, **38**(25), 10373.

21 L.H. Ai, X.Y. Gao, J. Jiang, *J. Power Sources*, 2014, **257**, 213.

22 G. Garbarino, P. Riani, M.A. Lucchini, F. Canepa, S. Kawale, G. Busca, *Int. J. Hydrogen Energy*, 2013, **38**(1), 82.

23 F. Baydaroglu, E. Özdemir, A. Hasimoglu, *Int. J. Hydrogen Energy*, 2014, **39**(3), 1516.

24 Y.C. Luo, T.H. Liu, Y. Hung, X.Y. Liu, C.Y. Mou, *Int. J. Hydrogen Energy*, 2013, **38**(18), 7280.

25 S. Gupta, N. Patel, R. Fernandes, D.C. Kothari, A. Miotello, *Int. J. Hydrogen Energy*, 2013, **38**(34), 14685.

26 Y.H. Chen, C.Y. Pan, *Int. J. Hydrogen Energy*, 2014, **39**(4), 1648.

27 H.J. Zhang, T. Watanabe, M. Okumura, M. Haruta, N. Toshima, *Nat. Mater.*, 2012, **11**(1), 49.

28 H.J. Zhang, T. Watanabe, M. Okumura, M. Haruta, N.Toshima, *J. Catal.*, 2013, **305**, 7.

29 J. Du, F.Y. Cheng, M. Si, J. Liang, Z.L. Tao, J. Chen, *Int. J. Hydrogen Energy*, 2013, **38**(14), 5768.

30 L.H. Ai, X.M. Liu, J. Jiang, *J. Power Sources*, 2014, **257**, 213.

31 S. Saha, V. Basak, A. Dasgupta, S. Ganguly, D. Banerjee, K. Kargupta, *Int. J. Hydrogen Energy*, 2014, **39**(22), 11566.

32 X.F. Wang, S.R. Sun, Z.L. Huang, H.J. Zhang, S.W. Zhang, *Int. J. Hydrogen Energy*, 2014, **39**(2), 905.

33 B.S. Li, S.H. Chan, *Int. J. Hydrogen Energy*, 2013, **38**(8), 3338.

34 H.J. Zhang, L.L. Lu, Y.L. Cao, S. Du, Z. Cheng, S.W. Zhang, *Mater. Res. Bull.*, 2014, **49**, 393.

35 M.A. Matin, J.H. Jang, Y.U. Kwon, *Int. J. Hydrogen Energy*, 2014, **39**(8), 3710.

36 M. Yurderi, A. Bulut, M. Zahmakiran, M. Kaya, *Appl. Catal. B-Environ.*, 2014, **160-161**(1), 514.

37 Z.L. Wang, Y. Ping, J.M. Yan, H.J. Wang, Q. Jiang, *Int. J. Hydrogen Energy*, 2014, **39**(10), 4850.

38 J. Tayal, B. Rawat, S. Basu, *Int. J. Hydrogen Energy*, 2011, **36**(22), 14884.

39 B. Delley, *J. Chem. Phys.*, 2000, **113** (18), 7756.

40 J.P. Perdew, K. Burke, M. Ernzerhof, *Phys. Rev. Lett.*, 1996, **77**, 3865.

41 X. Wang, X.J. Kong, Y. Yu, H. Zhang, *J. Phys. Chem. C*, 2007, **111**(10), 3836.

42 R. Salvati, A. Longo, G. Carotenuto, S. De-Nicola, G.P. Pepe, L. Nicolais, A. Barone, *Appl. Surf. Sci.*, 2005, **248**(1-4), 28.

43 H.L. Yue, Y.J. Hu, H.G. Huang, S. Jiang, B. Tu, *Spectrochim. Acta. A*, 2014, **130**, 402.

44 X.F. Wang, Z.L. Huang, L.L. Lu, H.J. Zhang, Y.L. Cao, Y.J. Gu, Z. Cheng, S.W. Zhang, *J. Nanosci. Nanotechnol.*, 2014, **14**, 1.

45 R. Chamoun, U.B. Demirci, Y. Zaatar, A. Khoury, P. Miele, *Int. J. Hydrogen Energy*, 2010, **35**(13), 6583.

46 S.G. Peng, X.J. Fan, J. Zhang, F.Y. Wang, *Appl. Catal. B-Environ.*, 2013, **140-141**, 115.

47 W.L. Wang, Y.C. Zhao, D.H. Chen, X. Wang, X.L. Peng, J.N. Tian, *Int. J. Hydrogen Energy*, 2014, **39**(28), 16202.

48 X.W. Zhang, J.Z. Zhao, F.Y. Cheng, J. Liang, Z.L. Tao, J. Chen, *Int. J. Hydrogen Energy*, 2010, **35**(15), 8363.

49 L. Tamašauskaitė-Tamašiūnaitė, A. Jagminienė, A. Balčiūnaitė, A. Zabielaitė, A. Žielienė, L. Naruškevičius, J. Vaičiūnienė, A. Selskis, R. Juškėnas, E. Norkus, *Int. J. Hydrogen Energy*, 2013, **38** (33), 14232.

50 H.J. Zhang, J. Okuni, N. Toshima, *J. Colloid. Interf. Sci.*, 2011, **354**(1), 131.

51 H.J. Zhang, N. Toshima, *J. Colloid. Interf. Sci.*, 2013, **394**, 166.

52 H.J. Zhang, N. Toshima, K. Takasaki, M. Okumura, *J. Alloy. Compd.*, 2014, **586**, 462.

Captions

Fig. 1 UV-Vis spectra of colloidal dispersions of Au, Co, Ni, $Ni_{50}Au_{50}$, $Ni_{50}Au_{30}Co_{20}$ and $Ni_{50}Au_{10}Co_{40}$ NPs ($[M^{n+}]$= 0.66 mM, R_{NaBH4}=5, R_{PVP}=100).

Fig. 2 TEM micrographs and size distribution histograms of Au, $Ni_{50}Au_{50}$, $Co_{50}Au_{50}$, $Ni_{50}Au_{30}Co_{20}$ and $Ni_{50}Au_{10}Co_{40}$ NPs ($[M^{n+}]$= 0.66 mM, R_{NaBH4}=5, R_{PVP}=100).

Fig. 3 HR-TEM image of as-prepared $Ni_{50}Au_{10}Co_{40}$ TNPs ($[M^{n+}]$ =0.66 mM, R_{NaBH4}=5, R_{PVP}=100).

Fig. 4 Comparison of catalytic activity of Au, Ni, Co, $Ni_{50}Au_{50}$, $Co_{50}Au_{50}$, $Ni_{50}Co_{50}$, $Ni_{50}Au_{30}Co_{20}$ and $Ni_{50}Au_{10}Co_{40}$ NPs ($[M^{n+}]$= 0.66 mM, R_{NaBH4}=5, R_{PVP}=100).

Fig. 5 UV-Vis spectra of colloidal dispersions of $Ni_{(50-x/2)}Au_{(50-x/2)}Co_x$ (x=10, 20, 30, 40) TNPs ($[M^{n+}]$= 0.66 mM, R_{NaBH4}=5, R_{PVP}=100).

Fig. 6 TEM micrographs and size distribution histograms of $Ni_{30}Au_{30}Co_{40}$, $Ni_{35}Au_{35}Co_{30}$, $Ni_{40}Au_{40}Co_{20}$ and $Ni_{45}Au_{45}Co_{10}$ TNPs ($[M^{n+}]$= 0.66 mM, R_{NaBH4}=5, R_{PVP}=100).

Fig. 7 Comparison of catalytic activity of $Ni_{(50-x/2)}Au_{(50-x/2)}Co_x$ (x=10, 20, 30, 40) TNPs ($[M^{n+}]$= 0.66 mM, R_{NaBH4}=5, R_{PVP}=100).

Fig. 8 Linear fit of ln$k$ to 1/T of $Ni_{45}Au_{45}Co_{10}$ catalyst for hydrogen generation from $NaBH_4$.

Fig. 9 Schematic illustration of electronic charge transfer effects in Ni/Au/Co TNPs.

Fig. 10 DFT calculations of electronic structure of $Ni_{25}Au_6Co_{24}$ TNPs (Ni atoms: the large light blue balls locate at top sites; Au atoms: the large yellow balls locate at face sites; and Co atoms: the small dark blue balls locate at edge sites).

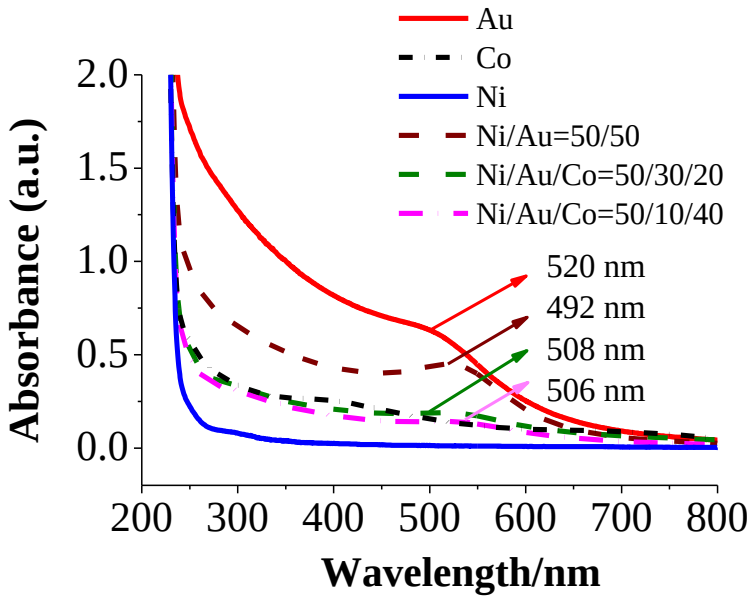

Fig. 1

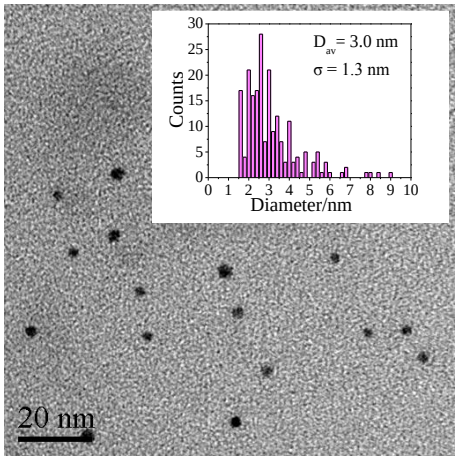

Au

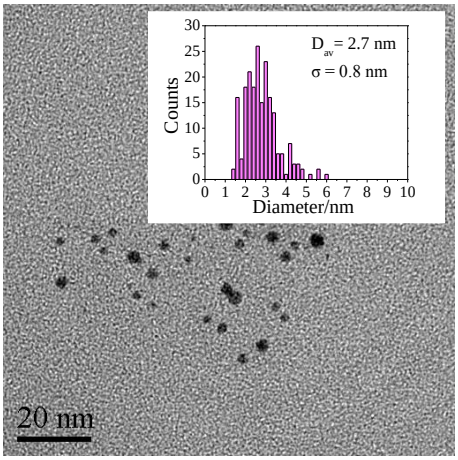

$Ni_{50}Au_{50}$

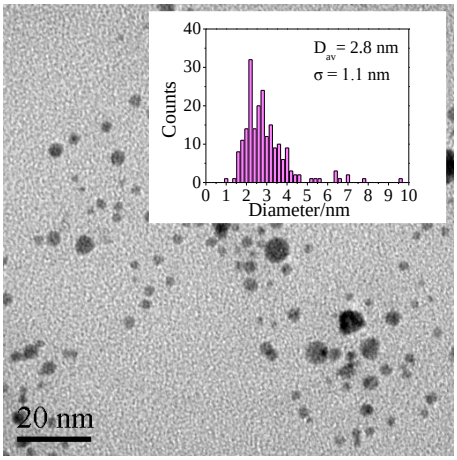

$Co_{50}Au_{50}$

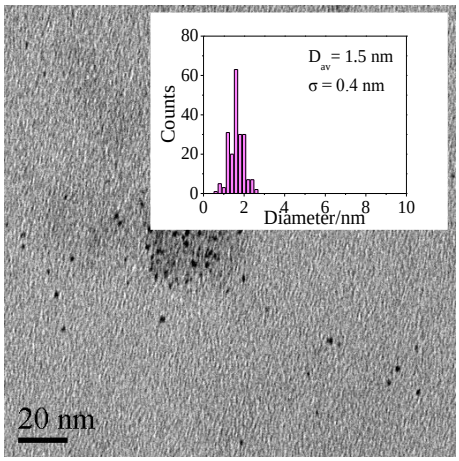

$Ni_{50}Au_{30}Co_{20}$

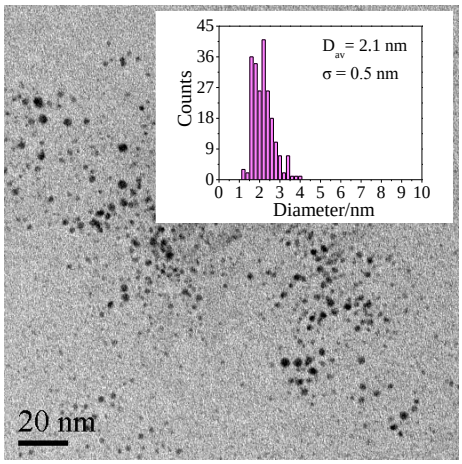

$Ni_{50}Au_{10}Co_{40}$

Fig. 2

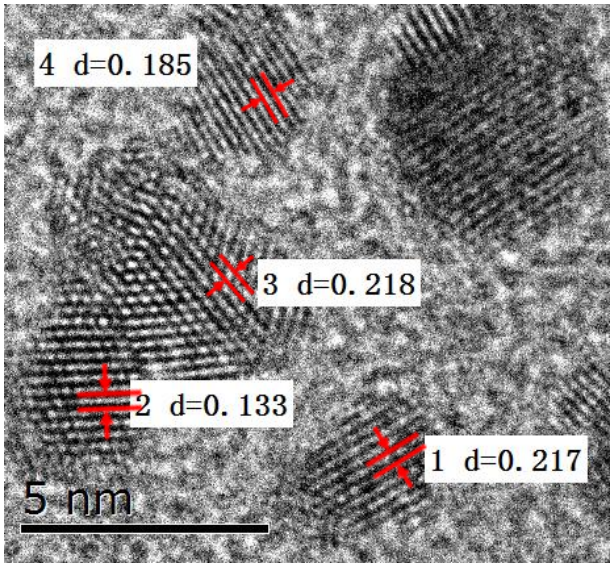

Fig. 3

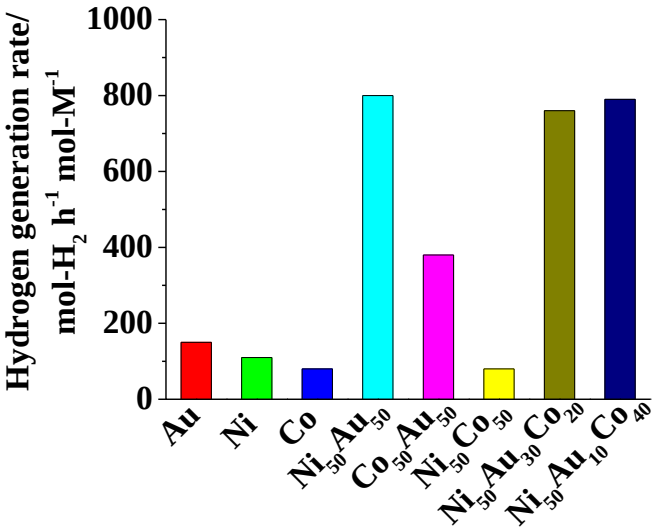

Fig. 4

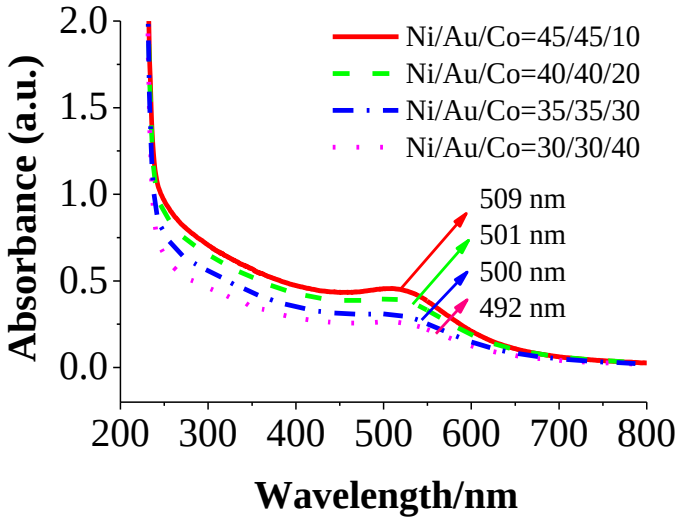

Fig. 5

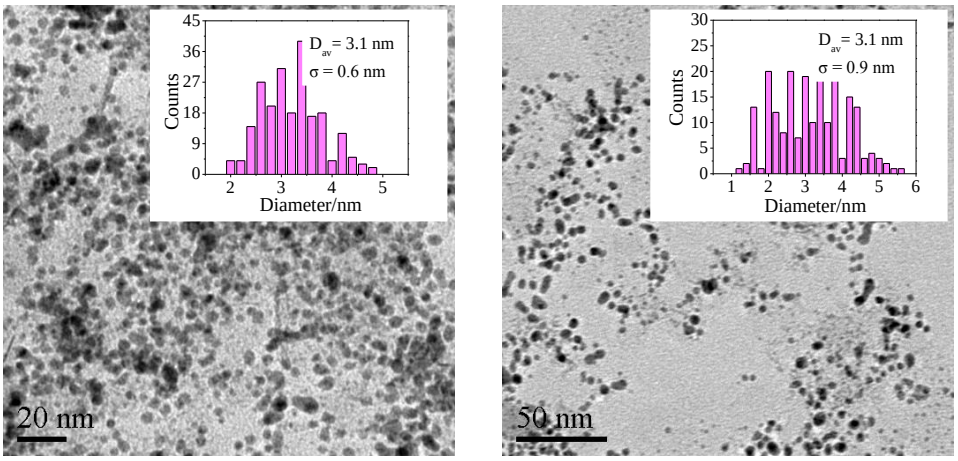

$Ni_{30}Au_{30}Co_{40}$ $Ni_{35}Au_{35}Co_{30}$

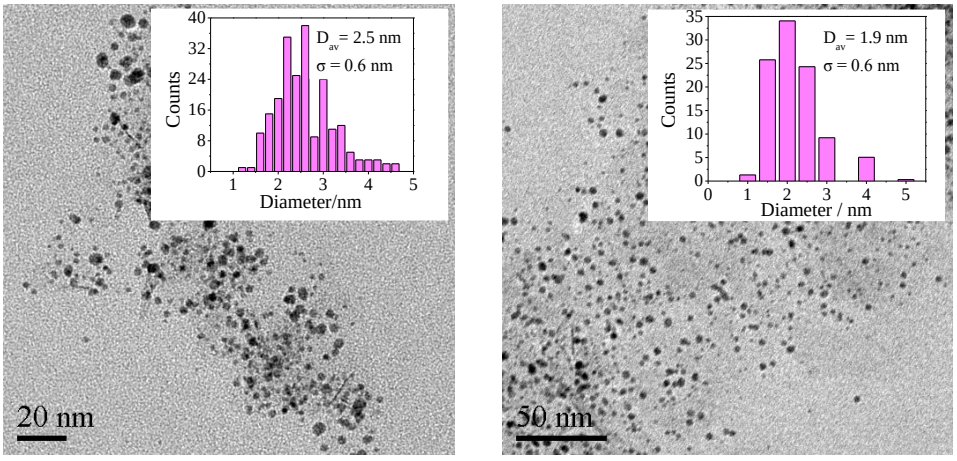

$Ni_{40}Au_{40}Co_{20}$ $Ni_{45}Au_{45}Co_{10}$

Fig. 6

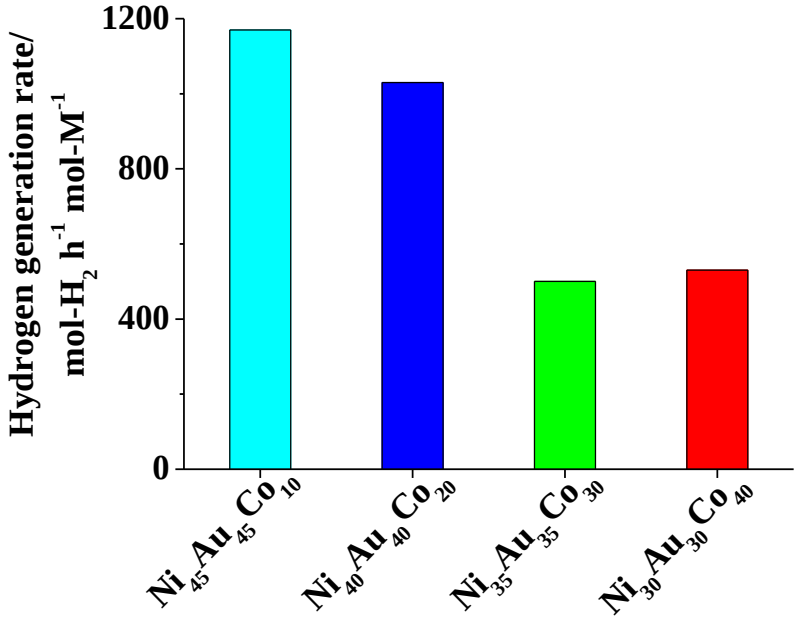

Fig. 7

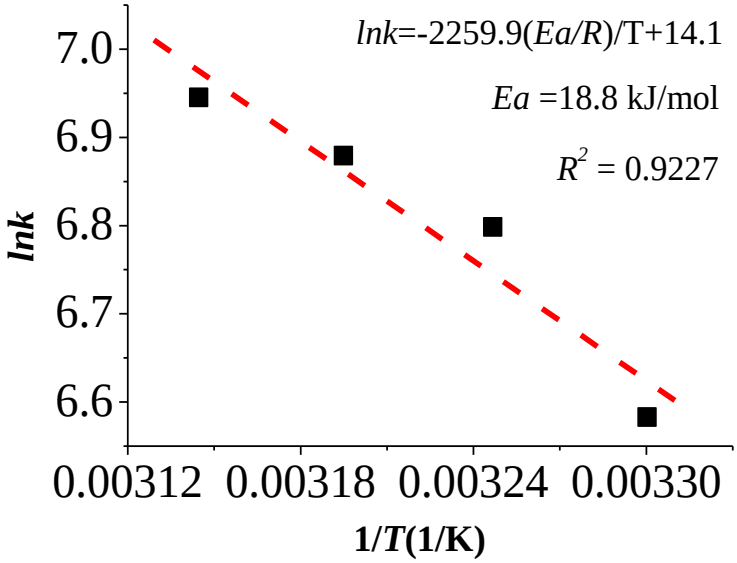

Fig. 8

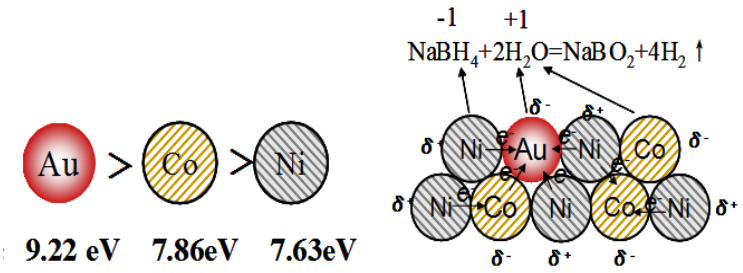

Fig. 9

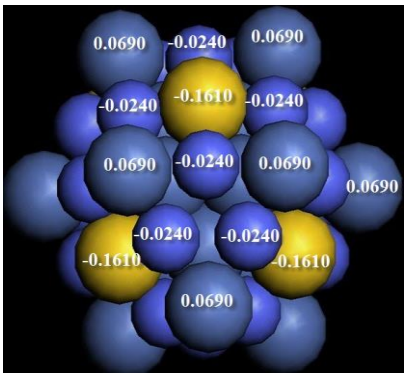

Fig. 10